Journal of Power Sources 267 (2014) 744–752

Contents lists available at ScienceDirect

Journal of Power Sources

journal homepage: www.elsevier.com/locate/jpowsour

Degradation diagnosis of aged $Li_4Ti_5O_{12}/LiFePO_4$ batteries

Rémi Castaing [a], Yvan Reynier [b], Nicolas Dupré [a, c], Donald Schleich [a, c], Séverine Jouanneau Si Larbi [b], Dominique Guyomard [a, c], Philippe Moreau [a, c, *]

[a] Institut des Matériaux Jean Rouxel (IMN), Université de Nantes, CNRS, 2 rue de la Houssinière, BP 32229, 44322 Nantes cedex 3, France
[b] CEA/DRT/LITEN/DEHT/LCPB, 17 rue des martyrs, 38054 Grenoble cedex 9, France
[c] Réseau sur le Stockage Électrochimique de l'Énergie (RS2E), FR CNRS 3459, France

HIGHLIGHTS

- $Li_4Ti_5O_{12}/LiFePO_4$ batteries exhibit huge capacity fade after 4–5 months of aging.
- Degradation explained using electrochemistry, spectroscopy and electron microscopy.
- Both positive and negative electrodes show no significant changes after aging.
- Capacity fade result from internal imbalance likely caused by parasitic reactions.

ARTICLE INFO

Article history:
Received 19 March 2014
Received in revised form
27 May 2014
Accepted 1 June 2014
Available online 9 June 2014

Keywords:
Lithium battery
Aging
Electric vehicle
End of charge/discharge slippage

ABSTRACT

$Li_4Ti_5O_{12}/LiFePO_4$ cells are cycled under 4 different conditions of discharge profile (galvanostatic or driving-based) and cycling rates (*C*/8 or 1*C*) during 4–5 months. All the cells exhibit capacity fade whose extent is not correlated with the aging condition. In order to understand aging phenomena, cells are disassembled at the end of cycle life and the recovered electrodes are analyzed using electrochemistry, electron microscopy, XRD and MAS-NMR. Positive and negative electrodes show no loss in active material and no change in electrochemical activity, active material structure and composite electrode structure. This rules out any irreversible electrode degradation. Lithium stoichiometry estimated by both XRD and electrochemistry is unexpectedly low in the positive electrode when the aging is stopped at full discharge. That indicates a loss of cyclable lithium or electrons leading to cell balancing evolution. That loss may have been caused by parasitic reactions occurring at both electrodes, in accordance with their rich surface chemistry as evidenced by MAS-NMR.

1. Introduction

In the past decade emphasis has been laid on developing durable lithium-ion batteries for electric vehicles. Current automotive industry needs extended energy and power supplies, as well as a high safety. It is however the cell longevity that is of major concern for electric transportation applications where lifetime up to 15 years is required [1]. It is therefore necessary to understand the performance decay of a battery subject to operating conditions that are typical of automotive application: complex cycling profile for electric vehicles, e.g. by Safari and Delacourt [2], continuous complex profile for hybrid electric vehicles, e.g. by Liaw et al. [3], as well as extended storage at different temperatures, e.g. by Kassem et al. [4]. Degradation mechanisms of the electrodes are generally divided into three families: (i) irreversible loss of active material, (ii) parasitic reactions leading to a loss of cyclable lithium or electrons, (iii) increase in resistance due to passive films formation and loss of contact [5–8]. Depending on the cell chemistry, i.e. the choice of active materials and of electrolyte salt and solvents, some degradation mechanisms overcome others. Since these electrode degradations manifest themselves under two macroscopic forms only: capacity fade and impedance rise, the degradation diagnosis cannot be fulfilled using electrochemical studies only, but also spectroscopic and microscopic studies are needed [9–12].

Amongst the numerous active materials referenced in the literature, it is possible to choose one that would meet the requirements of the target application, such as specific power and energy, lifetime, performance, safety and cost [1]. In the field of electric transportation, $Li_4Ti_5O_{12}$ and $LiFePO_4$ active materials have already been commercialized, notably for their attractive cyclability

* Corresponding author. Institut des Matériaux Jean Rouxel (IMN), Université de Nantes, CNRS, 2 rue de la Houssinière, BP 32229, 44322 Nantes cedex 3, France.
E-mail address: Philippe.Moreau@cnrs-imn.fr (P. Moreau).

http://dx.doi.org/10.1016/j.jpowsour.2014.06.002
0378-7753/

and their high level of safety: e.g. $LiFePO_4$ batteries and automobiles from Bolloré/Blue Solutions (France) and from BYD (China), $Li_4Ti_5O_{12}$ batteries from Tiankang (Hong-Kong) and from EIG (South Korea).

From the literature, degradation of $LiFePO_4$-containing cells mainly occurs at the negative electrode when the electrolyte becomes acidic, usually as $LiPF_6$ salt is hydrolyzed by traces of water: acidic species attack the active material and dissolve iron that will interfere with the SEI layer on the negative electrode [13–16]. Nevertheless, a few aging mechanisms have been exhibited on $LiFePO_4$ active material, such as the formation of surface layers containing LiF, lithium carbonates and lithium fluorophosphates [16–20]. On the negative electrode side, $Li_4Ti_5O_{12}$ is usually proposed to replace graphite, since its higher potential plateau (1.55 V) was thought to avoid the formation of the SEI. This is the reason why very few studies report the aging of $Li_4Ti_5O_{12}$: passivation layers are hardly detected on its surface [21–25].

The aim of this work is to understand the degradation mechanisms of a lithium-ion cell composed of $Li_4Ti_5O_{12}$/$LiFePO_4$ in $LiPF_6$/EC:DMC, in a specific cycling condition that is typical of automotive application. Very few reports deal with the aging of such a cell, since its capacity remains very stable upon cycling at room temperature (−0.008% per cycle at 1 C [26] or −0.003% per cycle at 5 C [27]) or fairly stable at high temperature (−0.14% per cycle at *C*/3 and 55 °C [13]). Whereas the causes for capacity fading were not explored in previous studies, we attempt to determine degradation mechanisms and analyze them using complementary electrochemical, spectroscopic and microscopic tools.

2. Experimental

2.1. Cell constitution

Experimental studies were performed on $LiFePO_4$/$Li_4Ti_5O_{12}$ Swagelok cells [20] with initial capacity *C* of 0.748 ± 0.010 mAh. This cell consists of a carbon-coated $LiFePO_4$ positive electrode with 1.0 mAh/cm^2 and a $Li_4Ti_5O_{12}$ negative electrode with 1.3 mAh/cm^2, both tape-casted onto an aluminium current collector; electrodes are 1 cm diameter discs. Electrolyte was a commercial (Novolyte) 1 mol L^{-1} solution of $LiPF_6$ in a mixture of EC and DMC with volumic ratio of 1; electrolyte was contained in two discs of glass fiber separator. The cells were assembled in an argon-filled glovebox.

All electrochemistry measurements were performed on a multichannel potentiostat/galvanostat VMP3 provided by BioLogic and monitored by the software EC-Lab.

2.2. Aging procedure

The cells were aged using 4 cycling conditions consisting in alternance of charges and discharges: reference mild, reference intensive, driving mild and driving intensive (respectively Rm, Ri, Dm and Di). Reference aging is a galvanostatic charge/discharge alternance, whereas driving aging consists of galvanostatic charges and complex discharges whose power profile was designed from United States Advanced Battery Consortium [28] as depicted in Fig. 1 (the FUDS profile was used as it is; only its amplitude was reduced to ensure an average power equivalent to the demanded *C*-rate); mild and intensive agings correspond to cycling rates of *C*/8 and 1*C* respectively. For each condition, 3 or 4 cells were aged. Charges and discharges were separated by 10 min relaxation periods. Voltage cut-offs for galvanostatic charges and discharges are respectively 2.5 V and 0.95 V.

Periodic (monthly) analyses were performed using reference performance tests. This test is made up of 5 galvanostatic charge/discharge cycles at increasing currents from *C*/25 to 2*C*; each cycle consists of CCCV charge (constant current constant voltage) up to 2.5 V and constant current discharge down to 0.5 V with relaxation periods until potential variation is less than 2 mV h^{-1}.

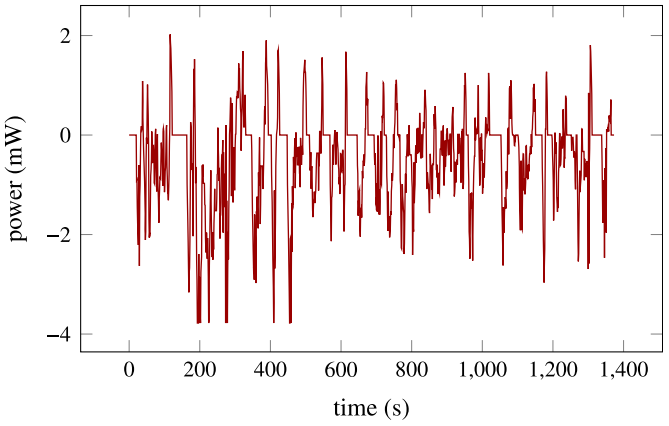

Fig. 1. FUDS profile from United States Advanced Battery Consortium (28) scaled to get an average power of 1*C*.

2.3. End of aging

After aging, the cell was discharged down to 0.5 V at 0.04 C then relaxed until the potential evolution was below 2 mV h^{-1}. For each group, corresponding to an aging condition, the cell 1 was devoted to half-cell study with the positive electrode while its negative electrode was analyzed using XRD. The cell 2 was devoted to half-cell study with the negative electrode while its positive electrode was analyzed using XRD. The cells 3 and 4 were used for NMR, SEM and TEM.

2.4. Half-cell study

One of the electrodes was removed from the cell while the other electrode was cycled in the same cell with a Li counter electrode; no electrolyte was added in order to avoid any rinsing of interphasial layers. This further cycling at *C*/25 consists of a charge then a discharge for positive electrodes and a discharge then a charge for negative electrodes. The second step permits to calculate intrinsic capacity, that is the ability of positive (negative) electrode to intercalate (desintercalate) lithium. The difference between first and second cycle leads to residual capacity, corresponding to the lack of lithium filling (the remaining lithium) in the positive electrode (in the negative electrode).

2.5. Electron microscopy

Scanning electron microscopy imaging was performed using a JEOL JSM 7600F microscope on (not rinsed) electrodes. Transmission electron microscopy imaging was performed using a FEG Hitachi HF2000 microscope operated at 200 kV. In that case, (not rinsed) electrodes were scraped off from the collector, dispersed in dimethyl carbonate using ultrasound, then deposited on a Holey carbon grid in ambient air.

2.6. X-ray diffraction

X-ray diffraction was performed using a Bruker D8 diffractometer in a Bragg-Brentano geometry, equipped with a copper anode, a germanium monochromator (Cu_{K-L3} = 1.540598 Å) and a LinxEye position sensitive detector. Diffractograms were acquired

directly on (not rinsed) electrodes coated on the current collector, this explains why reflections associated with aluminium are visible. The sample holder is an airtight cell made up of a PolyEtherEtherKetone globe and a silicon base. Sample preparation was made in argon-filled glovebox. Rietveld analysis was performed using the Jana software.

2.7. MAS-NMR

^{7}Li and ^{19}F MAS-NMR measurements were acquired on a Bruker Avance 500 spectrometer ($B_0 = 11.8$ T, Larmor frequency of ^{7}Li and ^{19}F are respectively 194 MHz and 470 MHz). The electrode was scraped off from the collector, not rinsed, dried under vacuum at room temperature for 10 h then filled into a cylindrical 2.5 mm diameter zirconia rotor. Sample preparation was made in argon-filled glovebox. ^{7}Li NMR was performed at a spinning rate of 25 kHz with a single pulse sequence, a pre-scan delay of 50 μs and a recycle time of 60 s; ^{19}F NMR was performed at a spinning rate of 23.5 kHz with a Hahn echo sequence, a pre-scan delay of 5 μs and a recycle time of 60 s. These analysis conditions were adapted from Dupré et al. [29] in order to separate surface signal from bulk signal, since MAS-NMR is used here to analyze surface species. In order to quantitatively compare spectra, they were normalized with respect to the mass of sample, the number of scans and the receiver gain. Spectra were filtered using Butterworth filter (order: 5, cut-off frequency: 0.12 ppm^{-1}).

3. Results

3.1. Electrochemical performance after aging

The capacity is periodically measured in reference tests in discharge at $C/25$. Its evolution during aging for each cycling condition is presented in Fig. 2.

Firstly, there is a continuous decrease in capacity and a 20% loss of capacity is experienced after 70 days on average. It is interesting to compare these capacity fading to those reported in the literature on the same system $LiFePO_4/Li_4Ti_5O_{12}$. In order to overcome the difference in cycling conditions, the lifetime duration is calculated: it corresponds to the time to lose 20% of capacity. This lifetime is extrapolated taking into consideration the actual discharge and charge duration and not the theoretical one, thanks to the Ragone plot if given. The lifetime of such a system is then 525 days for Zaghib et al. [30], 208 days for Franger et al. [26] and 87 days for Jaiswal et al. [27]. The lifetime in this work is close to Jaiswal's result. There is however a discrepancy in capacity retention amongst all studies of this system. This will be discussed further in the discussion section.

Secondly, taking into account the error bars, it is clearly not possible to draw a conclusion about the influence of aging condition on the degradations. The large discrepancy of capacity evolution amongst each group means there is a lack of reproducibility. This may come from the cell assembly process, since Swagelok cell assembly is subject to variability due to its components (spring, plunger …). The quality of electrolyte (batch number, freshness …) has also an influence on the aging rate.

Fig. 3 presents the evolution of potential–charge profiles measured during reference performance test cycles. It highlights a fade of capacity without an increase in polarization as the plateau potential remains the same at $C/2$. The absence of increase in polarization is an indication of the conservation of good electronic and ionic conductions within the composite electrode. This observation may thus rule out a hypothesis of degradation of the composite electrode. Moreover, a low increase in internal resistance was measured at the end of aging: 44 ± 9% in average amongst all the cells. This shows electrodes are only slightly passivated.

3.2. Half-cell study

At the end of aging (i.e. after 4–5 months), one of the electrodes was cycled versus a lithium counter electrode in order to have access to both its intrinsic and residual capacity [10,31].

3.2.1. Intrinsic capacities

Intrinsic capacity is related to the amount of active material in the electrode. Charge or discharge profiles of electrodes in half-cells are presented in Fig. 4. Only a small change in capacity and plateau potential is visible. This indicates that the electrodes have almost the same electrochemical activity in spite of the aging.

In Table 1, intrinsic capacities are compared before and after aging. One observes no significant difference between intrinsic capacity of aged electrodes in half-cells and intrinsic capacity of fresh electrodes. These results mean that only a negligible amount of active material has been lost during aging, either due to corrosion or due to disconnection from the percolating network.

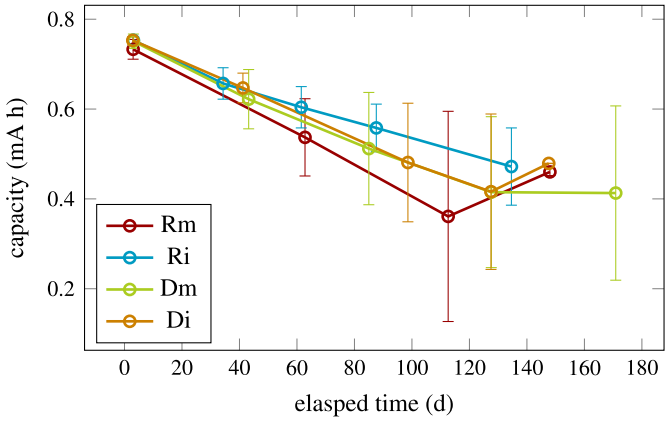

Fig. 2. Fade of capacity during aging measured as the mean of all the cells from each of the four cycling conditions: Rm, Ri, Dm and Di. Each mark corresponds to a reference performance test. Error bars depicted correspond to standard deviation amongst the group.

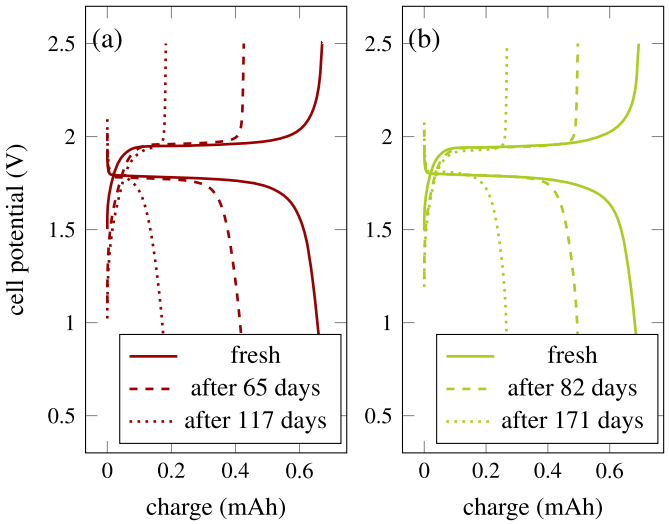

Fig. 3. Evolution of charge/discharge profiles measured at $C/2$ for fresh cells (solid line), at middle-of-life (dashed line) and at end of life (dotted). (a) Aging performed in Rm condition (cell 3), (b) aging performed in Dm condition (cell 1).

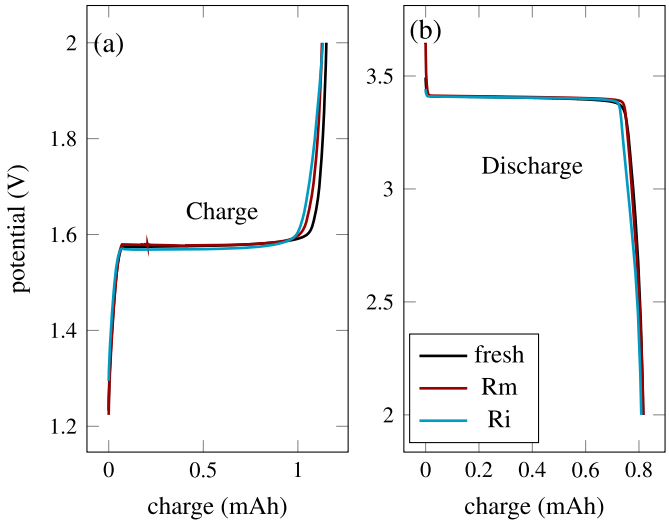

Fig. 4. Charge or discharge profile of half-cells measured at *C*/25 for fresh and aged electrodes. (a) Half-cell with $Li_4Ti_5O_{12}$ electrode in charge (cell 2), (b) half-cell with $LiFePO_4$ electrode in discharge (cell1).

Table 1
Intrinsic and residual capacities in mAh of $LiFePO_4$ and $Li_4Ti_5O_{12}$ electrodes in half-cells. Confidence intervals for fresh values are given, since this measurement was repeated. The values after aging come from a single cell for each group. NA means "not applicable" because the measurement failed due to software issue during recording process.

Capacity	Fresh	Rm	Ri	Dm	Di
$Li_4Ti_5O_{12}$ electrode (cell 2)					
Intrinsic	1.13 ± 0.16	1.13	1.13	1.18	1.03
Residual	−0.092 ± 0.039	−0.047	−0.078	−0.100	NA
$LiFePO_4$ electrode (cell 1)					
Intrinsic	0.796 ± 0.054	0.816	0.802	0.781	0.823
Residual	0.009 ± 0.010	0.406	0.408	NA	0.624

3.2.2. Residual capacities

Residual capacity corresponds to the amount of empty (occupied) sites left in the $LiFePO_4$ ($Li_4Ti_5O_{12}$) framework when the full cell is fully discharged. It is an indication for cyclable lithium or electron loss because of side reactions, thus leading to a continuously less intercalated (desintercalated) electrode at the end of discharge. Apart from the negative values in $Li_4Ti_5O_{12}$ that can simply be explained by the passivation of the fresh lithium counter electrode during the first cycle, significant residual capacities in $LiFePO_4$ indicate that the positive electrode is not fully lithiated when the full cell is discharged at the end of life (see Table 1). The lack of lithium intercalation at the end of aging is observed on the positive side since the half-cell study was done at a discharged state. Theses results indicate that the capacity fade could be attributed to a slippage of the electrodes reducing progressively their stoichiometry window.

3.3. Microscopy studies

After the half-cell study, electrodes were harvested and their microstructure was characterized using microscopy. SEM imaging did not allow to observe any change in texture, particle size and homogeneity. This result indicates composite electrode morphology is not degraded after aging and remains homogeneous. TEM imaging was then performed to compare $Li_4Ti_5O_{12}$ and $LiFePO_4$ grains between fresh and aged states. The pictures are showed in Fig. 5. It is worth noting that the electrode was dispersed in a solvent before analysis, so that each grain could be separately visible. Any surface layer due to electrolyte decomposition is however not expected to be seen because of this rinsing.

No evidence of change in $Li_4Ti_5O_{12}$ grains is observed in images (a) to (d). By looking at images (a) and (b), grain shape and particle size – from 40 nm to 100 nm – are conserved. Images (c) and (d) show that crystalline planes are still visible after aging. By comparing images (e) and (f), $LiFePO_4$ grains are found similar in terms of particle shape and particle size: ranging from 70 nm to 200 nm. Images (g) and (h) reveal that the high crystallinity is conserved throughout aging. Those results indicate active grains of

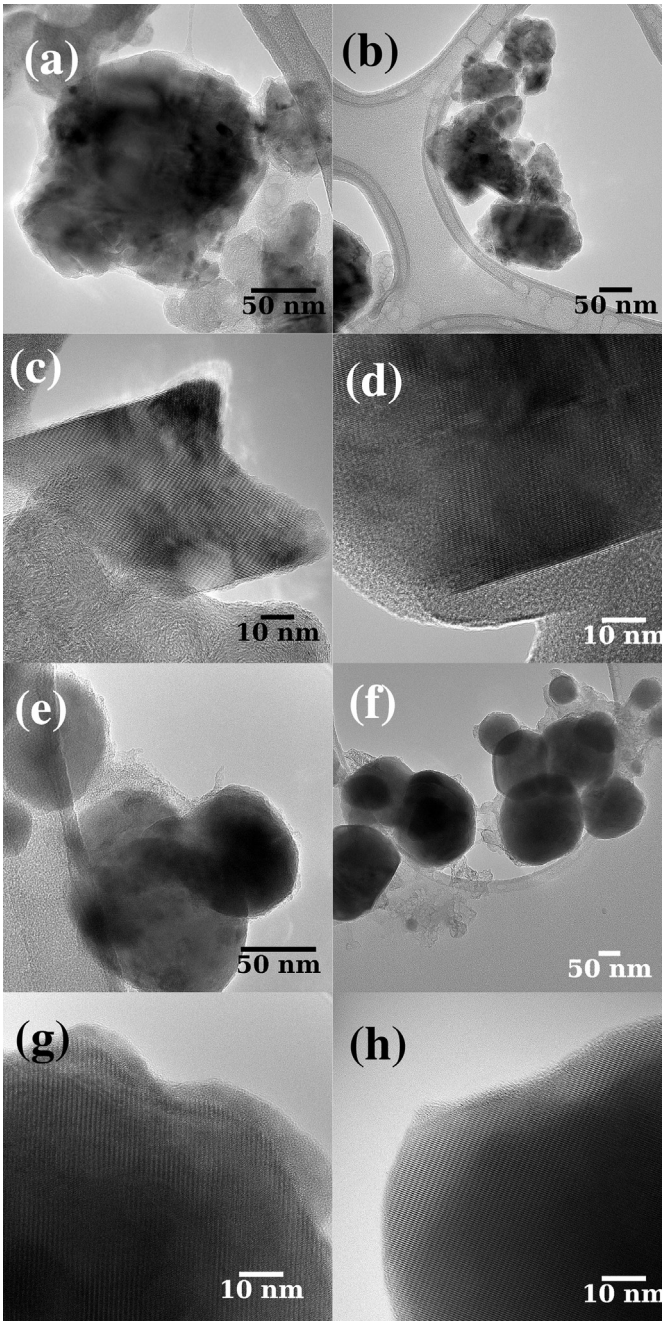

Fig. 5. TEM and high-resolution TEM images of grains of $Li_4Ti_5O_{12}$ (a–d) and $LiFePO_4$ (e–h) electrodes. Fresh electrodes (left column: a, c, e, g) and aged electrode from cell Ri3 (right column: b, d, f, h) are compared in terms of particle distribution and crystallinity.

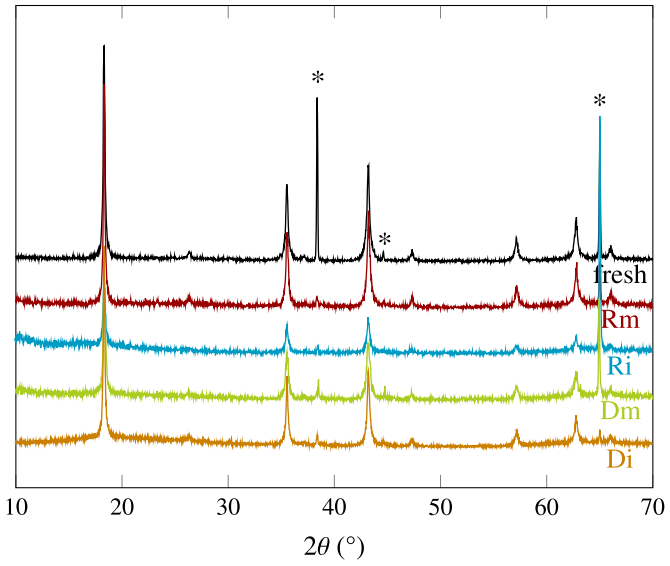

Fig. 6. XRD patterns of $Li_4Ti_5O_{12}$ electrodes from cells 2. Stars indicate reflections associated to aluminium current collector.

both $Li_4Ti_5O_{12}$ and $LiFePO_4$ do not suffer from electrochemical aging.

3.4. XRD measurements

XRD patterns in Figs. 6 and 7 were acquired on both electrodes for each aging (Rm, Ri, Dm and Di). No significant change is observed in the global patterns, in agreement with the analysis of cycled $LiFePO_4$ electrodes by Maccario et al. [32]. However, in the case of the positive electrode, after aging new peaks associated to $FePO_4$ are detected. The presence of the delithiated phase indicates that positive electrodes are not completely intercalated with lithium at the end of cell discharge.

All diffractograms were refined with Rietveld analysis and results are reported in Table 2: the lattice parameters, the lithium stoichiometry in the positive electrode and the crystallite size.

3.4.1. Lattice parameters of active materials

As reported in Table 2, only little variation of lattice parameters of both active materials can be detected after aging. That result confirms the hypothesis of an absence of significant active material degradation.

3.4.2. Lithium stoichiometry in positive electrodes

From XRD patterns of $LiFePO_4$ electrodes it is possible to estimate the lithium stoichiometry by calculating phase ratio between $LiFePO_4$ and $FePO_4$ (see Table 2). As explained previously, after aging positive electrodes are not completely filled with lithium.

3.4.3. Crystallite size

A slight broadening of peaks can be observed in Figs. 6 and 7 only in the case of positive electrodes. By taking into account the whole pattern, crystallite size is evaluated with absence of microstrains (see Table 2). Confirming the observation of peak broadening, there is significant evolution in crystallite size in the positive electrode. This evolution is a decrease that is further intensified at higher currents, by comparison of aging conditions Di and Ri with conditions Dm and Rm. Electrochemical grinding could be accountable for that decrease in crystallite size, but this seems not to be detrimental to active material electrochemical activity, since intrinsic capacity is preserved (see Table 1).

3.5. Surface chemistry using MAS-NMR

Surface chemistry on positive and negative electrode grains is analyzed using MAS-NMR for ^7Li and ^{19}F nuclei. ^7Li spectra in Fig. 8 show a unique, broad resonance at about 0 ppm that is typical of diamagnetic lithium [29]. It is assigned to lithium present in surface layers and not to paramagnetic lithium intercalated in the positive electrode, found at −8 ppm by Tucker et al. [33], since acquisition conditions allow to separate surface and bulk signals. Actually this diamagnetic signal corresponds to an overlapping of different signals coming from the diamagnetic lithium species present at the surface (Li_2CO_3, LiF, Li_2O, $LiPF_6$, other lithiated carbonates, etc.); unfortunately it is not possible to differentiate these species with ^7Li spectra only, because of the narrow chemical shift range of diamagnetic lithium.

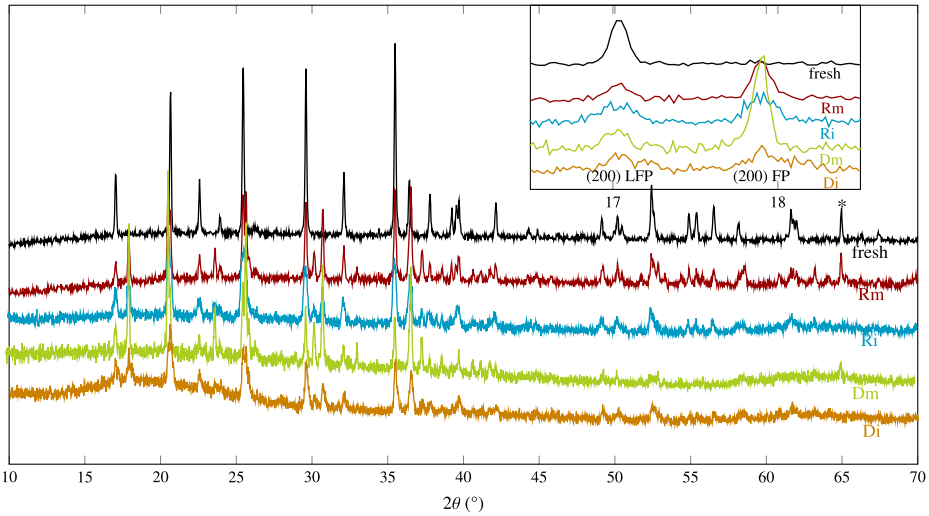

Fig. 7. XRD patterns of $LiFePO_4$ electrodes from cells 1. The star indicates the reflection associated to aluminium current collector. Inset shows the (200) reflection for $LiFePO_4$ and $FePO_4$ phases.

Table 2
Refinement results from XRD patterns of fresh and aged electrodes. The values come from a single cell for each group; errors were calculated from the goodness of refinement. $LiFePO_4$ and $FePO_4$ phases from positive electrodes are indexed in the orthorhombic Pnmb space group. $Li_4Ti_5O_{12}$ phase from negative electrodes is indexed in the cubic Fd-3m group. Refinement results include the mean crystallite size, the lattice parameters and the lithium stoichiometry in the positive electrode, corresponding to the $LiFePO_4/(LiFePO_4 + FePO_4)$ molar ratio, as well as the *R*-factor R_{wp}.

	Fresh	Rm	Ri	Dm	Di
Negative electrode (cell 1)					
crystallite size (nm)	31 ± 2	41 ± 2	38 ± 2	32 ± 1	39 ± 2
$Li_4Ti_5O_{12} - a$ (Å)	8.3637 (12)	8.3583 (14)	8.3634 (16)	8.3674 (14)	8.3600 (14)
R_{wp} (%)	18.8	22.7	19.9	22.1	17.5
Positive electrode (cell 2)					
crystallite size (nm)	130 ± 13	99 ± 2	57 ± 11	108 ± 3	68 ± 16
$LiFePO_4 - a$ (Å)	6.0076 (3)	6.0061 (6)	6.0110 (14)	6.0052 (14)	6.0021 (13)
$LiFePO_4 - b$ (Å)	10.328 (1)	10.325 (1)	10.334 (2)	10.322 (3)	10.324 (2)
$LiFePO_4 - c$ (Å)	4.6933 (3)	4.6932 (6)	4.6975 (13)	4.6929 (12)	4.6908 (12)
$FePO_4 - a$ (Å)	–	5.7946 (5)	5.7976 (14)	5.7931 (7)	5.7923 (15)
$FePO_4 - b$ (Å)	–	9.827 (1)	9.829 (3)	9.824 (2)	9.820 (3)
$FePO_4 - c$ (Å)	–	4.7843 (6)	4.7855 (13)	4.7830 (7)	4.7829 (16)
Li stoichiometry	1	0.505 ± 0.030	0.673 ± 0.045	0.315 ± 0.030	0.613 ± 0.036
R_{wp} (%)	6.38	7.78	9.47	12.62	8.06

^{19}F spectra in Fig. 9 allow the detection of diamagnetic fluorinated species. Consequently resonances associated with $LiPF_6$ and LiF are observed at −72 ppm and −204 ppm respectively [34]. Other lithium fluorophosphates are also detected on negative electrodes typically between −76 ppm and −84 ppm [35].

The combination of ^7Li and ^{19}F spectra shows that both electrodes developed a rich surface chemistry during aging, including lithiated and fluorinated species, amongst which LiF is majority. The presence of $LiPF_6$ in several spectra may originate from electrolyte salt remaining in the electrode porosity, which was not rinsed before analysis. This surface chemistry on the $LiFePO_4$ electrode is consistent since a comparable result was evidenced using both MAS-NMR and XPS after soaking $LiFePO_4$ active material in $LiPF_6$-based electrolyte [20].

4. Discussion

Prior work has documented causes for the fade of performance of lithium-ion batteries. They are generally divided into three families: irreversible loss of active material, reversible loss of cyclable lithium or electrons, rise of impedance [5–8]. The purpose of this study was to provide information on the aging of the $Li_4Ti_5O_{12}/LiFePO_4$ in $LiPF_6$/EC:DMC system with respect to degradation mechanisms referenced in the literature.

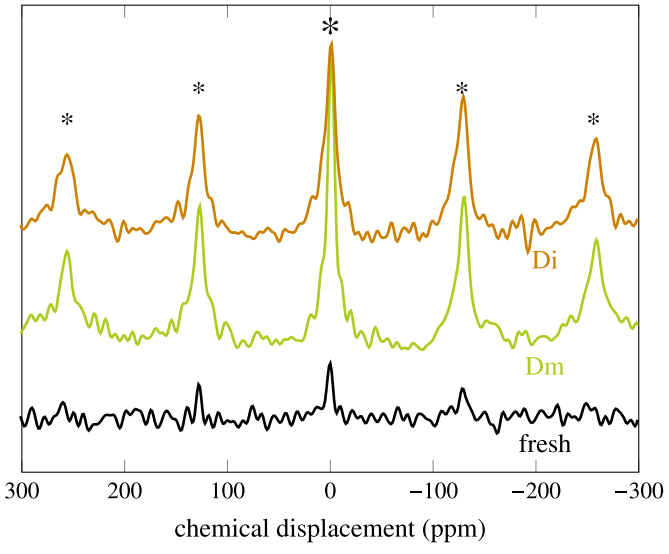

Fig. 8. ^7Li MAS-NMR spectra on $LiFePO_4$ electrodes (cells 3) showing isotropic resonance at 0 ppm corresponding to diamagnetic lithiated species. Isotropic resonance and its spinning sidebands are marked with respectively large and small stars.

The results section reported a discrepancy in the capacity retention between the cells of this study and those described in the literature [26,27,30]. On the one hand, explanations can be found regarding the measurement of capacity. First of all, the capacity is not measured the same way: whereas in the previous studies it is measured during each cycle, under stress conditions and at high rate (at least 1*C*), in the present study the cycling was stopped and a reference test was performed to have access to the *C*/25 capacity, which is considered as the maximal available capacity [2]. Secondly, cell-to-cell variability requires to repeat the experiment (3 times in this study), so that an average and representative value is presented. No statistical study is reported in the works of Franger et al. [26], Zaghib et al. [30]. For these reasons, no straightforward comparison can be made with the previous ones.

On the other hand, a difference in experimental conditions may also cause a difference in the capacity retention. For instance, changing the cell design – coin, Swagelok, pouch, coffee-bag, commercial, etc. – may modify the current distribution inside the battery [36] or its permeability to ambient air and moisture [37], leading to a different performance retention. It may thus be argued that Swagelok cells can suffer from a lack of airtightness that leads to electrolyte leakage or air intrusion. However, in an additional work, this hypothesis was discarded by comparing the calendar aging of cells left in ambient air (capacity loss rate of 1.95 ± 0.24 μA h d^{-1}) with cells sealed in a plastic bag inside an argon-filled glovebox (1.77 ± 0.02 μA h d^{-1}). Secondly, it is worth noting that Swagelok architecture allows the use of higher quantity of electrolyte: 0.4 mL. This may increase the amount of loss due to parasitic reactions involving the electrolyte, because of the high electrolyte/electrode mass ratio [15,16]. Moreover, the use of larger volume of electrolyte may shift the saturation equilibrium and allow further dissolution of surface species coming from these parasitic reactions; the active material surface is then free to experience new parasitic reactions. Thirdly, it has been observed in our lab that electrolyte with the same stated composition but coming from different manufacturers leads to a difference in capacity retention. Average lifetime of a $Li_4Ti_5O_{12}/LiFePO_4$ cell was 70 ± 14 days for a manufacturer and 145 ± 9 days for another one (errors are calculated using Student law). Other studies of the effect of the presence of contaminants in the electrolyte, such as moisture, are reported in the literature [38,39]. At last, all the

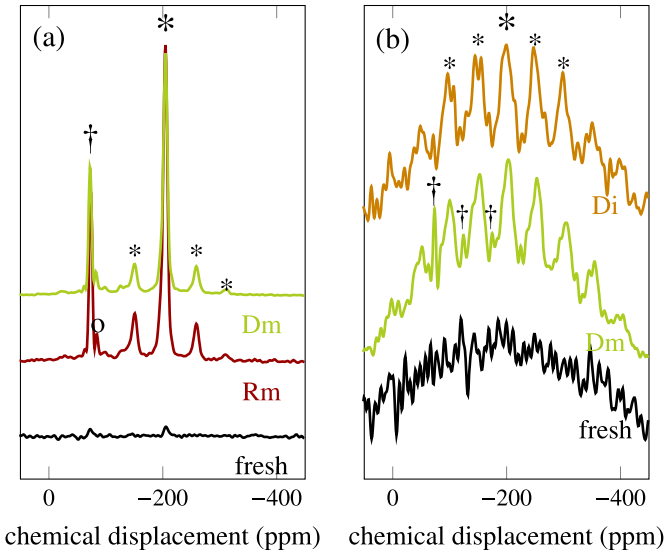

Fig. 9. ^{19}F MAS-NMR spectra on $Li_4Ti_5O_{12}$ (a) and $LiFePO_4$ (b) electrodes (cells 3 or 4). The spectra show isotropic resonances at −76 ppm, −80 ppm and −204 ppm corresponding to $LiPF_6$, other lithium fluorophosphates and LiF respectively. Isotropic resonances and their spinning sidebands are marked with dags, circles and stars, for $LiPF_6$, the other fluorophosphates and LiF respectively (a large symbol for the isotropic resonance and small symbols for its spinning sidebands).

electrolyte-driven parasitic reactions may be strongly influenced by the pressure applied to the separator and the electrodes – using a spring in Swagelok architecture. Apart from these points, electrode formulation [40] as well as electrode balancing in the cell [6] have to be considered before any comparison. In conclusion, it is obvious that experimental conditions have an effect on the degradation mechanisms. By changing the experimental conditions, the balance between the three main aging mechanisms is modified: loss of active material, loss of cyclable lithium or electrons, rise of impedance. A change in the combination of these chemical and mechanical processes leads to a different performance evolution. This explains why capacity fading rate can be different on the same electrochemical system using different experimental conditions. In present work, the experimental conditions seem to have favored the loss of cyclable lithium or electrons as main aging cause: this finding is developed below.

The results section reported that after aging positive and negative electrodes still have the same aspect, the same electrochemical performance and very similar active material structure. This was proven using electrochemistry on half-cells containing each electrode, as well as spectroscopic and microscopic tools. This shows the absence of degradation in the composite electrode, i.e. both electrodes can be separately used as fresh ones after aging of the cell.

Positive electrodes were found to be partially lithiated at the end of discharge of the complete cell, whereas negative electrodes were at a fully delithiated state, as demonstrated by residual capacities and XRD phase attribution. Lithium stoichiometry y in Li_yFePO_4 can be obtained from two separate ways: as the difference between intrinsic and residual capacities over the intrinsic capacity, using half-cell study, and as phase ratio between $LiFePO_4$ and $FePO_4$ from XRD data. The stoichiometries were calculated on a different cell for each way; unfortunately, because of low reproducibility—as showed by error bars in Fig. 2 – they are not directly comparable to each other. Both are reported in Table 3, as well as the final state of health. Final state of health is the percentage ratio of final capacity over initial capacity, both measured in discharge at $C/25$. It is worth noting that the y value is always less than the final state of health. In the case of stoichiometry obtained from half-cell cycling (in cell 1), this can be explained by SEI formation on the fresh lithium counter electrode during the discharge in half-cell. Since the discharge capacity is over-estimated, the calculated y value is under-estimated. In the case of stoichiometry obtained from XRD (in cell 2), this can be explained by the fact electrodes were stored, neither rinsed nor dried, in the glovebox for some time before XRD analysis. In the meanwhile, a parasitic oxidation of Li_yFePO_4 (y about 0.5), caused by an unavoidable air or water contamination in such conditions, may lead to the lowering of the measured y value [41].

There is good agreement between lithium stoichiometry y in Li_yFePO_4 and the state of health at the end of life (for each of the two stoichiometry calculations, accordance is proven with less than 10% of error using tests on Pearson correlation coefficient). That last result is a proof that final state of health corresponds to an internal cell imbalance, as defined by Christensen and Newman [6] and Harlow et al. [42]. This imbalance appears as electrode capacity ranges are progressively shifting with respect to each other.

Table 3
Comparison between the lithium stoichiometry y in Li_yFePO_4 and the state of health at the end of life *SoH*. Lithium stoichiometries were extracted from two different cells using residual capacity (cell 1) or XRD (cell 2). Errors on y from cells 2 were calculated from the goodness of XRD refinement. NA means "not applicable" because the measurement failed due to software issue during recording process.

Cell	Fresh	Rm1	Rm2	Ri1	Ri2	Dm1	Dm2	Di1	Di2
SoH (%)	100	64.3	60.1	53.0	74.7	39.9	34.3	28.0	64.8
y (%)	100	50.2	51 ± 3	49.2	67 ± 5	NA	32 ± 3	24.2	61 ± 4

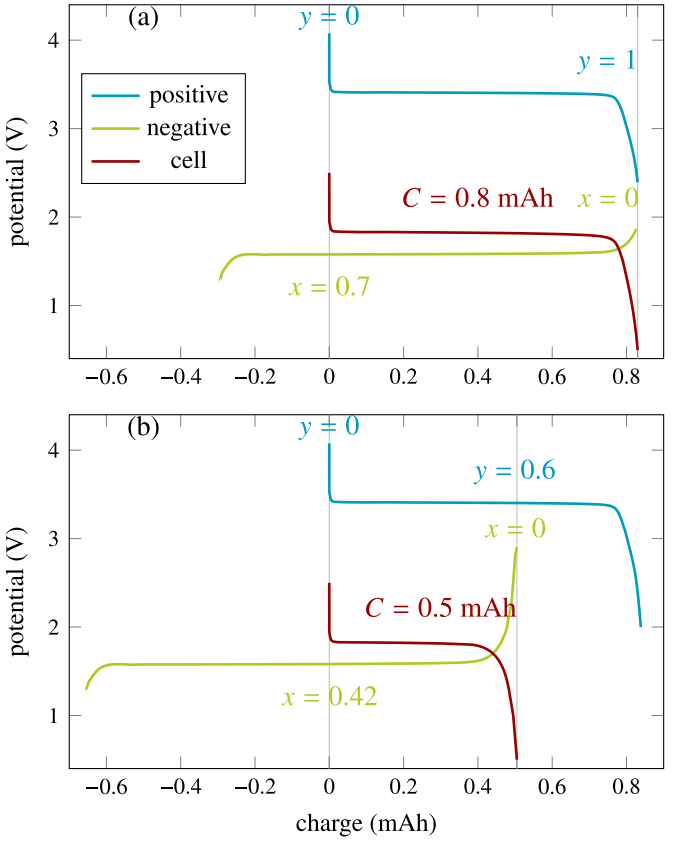

Fig. 10. Model of electrode slippage with lithium stoichiometries x in $Li_{4+3x}Ti_5O_{12}$ and y in Li_yFePO_4. Cell capacity in discharge C is defined between 2.5 V and 0.5 V. Electrode slippage is simulated between the fresh cell (a) and the aged cell Rm2 after 155 days (b).

Therefore the cause of capacity fade must be related to cell imbalance.

To help in figuring the evolution of internal balancing, Fig. 10 presents a model of electrode slippage. This model explains capacity fade only by a loss of cyclable lithium, since neither loss of active material nor increase in electrode polarization was observed [7,43,44]. Lithium stoichiometry in $LiFePO_4$ at the end of full-cell discharge is used to set the relative position of the typical curves of positive and negative electrodes. Then the typical curve of the full cell is calculated as the difference between positive and negative potential, with cut-offs of 2.5 V and 0.5 V. It is possible to determine the cell capacity C in discharge, as well as the stoichiometry in $Li_4Ti_5O_{12}$ at the end of full-cell charge, as explained by Kassem and Delacourt [10]. After aging in Rm condition after 155 days, electrodes have slipped about 0.3 mAh, leading to an internal imbalance that forces the positive electrode to cycle between $Li_{0.6}FePO_4$ and $FePO_4$ and the negative electrode to cycle between $Li_4Ti_5O_{12}$ and $Li_{5.3}Ti_5O_{12}$. The cell capacity measured at the end of aging is therefore only 0.5 mAh.

A possible origin for electrode slippage may be electron or lithium consumption in parasitic side reactions. After each cycle, part of the electrons exchanged between the electrodes is missing, because of parasitic reactions consuming electrons, lithium ions or both. This behavior is observed when coulombic efficiency is below 100% [45]. Such reaction paths can be brought out when the surface of the electrode is analyzed after cycling or soaking in the electrolyte using XPS and PES [9,16–20,46–48] NMR [20,49,50], FTIR and Raman [19,46,47] and ICP 16. Below are reported from the literature several parasitic reactions occurring in the presence of $LiPF_6$, EC:DMC electrolyte. They include organic solvent degradation and polymerization:

$$EC + 2e^- + 2Li^+ \rightarrow Li_2CO_3(s) + C_2H_4(g) \quad (1)$$

$$2EC + 2e^- + 2Li^+ \rightarrow (CH_2OCO_2Li)_2(s) + C_2H_4(g) \quad (2)$$

$$2EC + 2e^- + 2Li^+ \rightarrow LiOCO_2(CH_2)_4OCO_2Li(s) \quad (3)$$

$$DMC + e^- + Li^+ \rightarrow CH_3OLi(s) + CH_3OCO^{\bullet} \quad (4)$$

$$nEC + RO^- \rightarrow RO(CH_2CH_2OCO_2)_{n-1}CH_2CH_2OCO_2^- \quad (5)$$

The lithium salt $LiPF_6$ is in equilibrium, according to:

$$LiPF_6 \leftrightarrow LiF + PF_5 \quad (6)$$

However it can be either hydrolyzed by the moisture present in electrode porosity, or reduced:

$$LiPF_6 + H_2O \leftrightarrow LiF + POF_3 + 2HF \quad (7)$$

$$LiPF_6 + xe^- + xLi^+ \rightarrow xLiF + LiPF_{6-x} \quad (8)$$

$$PF_6^- + 2e^- + 3Li^+ \rightarrow 3LiF + PF_3 \quad (9)$$

In parallel its decomposition products can be hydrolyzed or reduced in their turn:

$$PF_5 + H_2O \rightarrow 2HF + POF_3 \quad (10)$$

$$PF_5 + 2xe^- + 2xLi^+ \rightarrow xLiF + Li_xPF_{5-x} \quad (11)$$

$$POF_3 + 2xe^- + 2xLi^+ \rightarrow xLiF + Li_xPF_{3-x}O \quad (12)$$

At the surface of the electrodes aged in this study, NMR-MAS revealed the presence of lithium diamagnetic species, amongst which LiF, $LiPF_6$ and other lithium fluorophosphates were indubitably detected. However, lithiated organic species such as lithium alkoxides could not be discriminated apart from other lithium diamagnetic species. This rich surface chemistry is in accordance with some of the parasitic reaction paths found in literature, which may explain the electrode slippage that was demonstrated. It is worth noting that these surface species are expected to develop either a thin or a heterogenous surface layer, since the polarization of the cell and of the separate electrodes did not increase significatively.

It has been shown in previous works (using XPS, MAS-NMR, SEM and TEM) that the SEI film on positive electrodes is not under the form of a thick, homogeneous layer on the active material grains [17,18,49,51]. This heterogeneous film is not resistive, as proven by EIS measurements. Therefore cells do not experience electrode polarization. Besides, products of the parasitic reactions mentioned in the text may either be deposited on the surface of electrode grains or remain in the electrolyte solution as a soluble species. In the latter case, no electrode polarization is expected.

A quantification of the surface species will benefit to a better understanding of their formation; furthermore it will allow the establishment of a more specific chemical model for the system studied here, i.e. $Li_4Ti_5O_{12}$/$LiFePO_4$ in $LiPF_6$/EC:DMC. This work is currently in progress thanks to a calibration of NMR-MAS spectra for positive and negative electrodes, as demonstrated by Cuisinier et al. [49].

Another possible origin for electrode slippage could be the inhomogeneous reaction in $LiFePO_4$. In a recent paper it is reported that some grains in $LiFePO_4$ electrode have priority over lithiation or delithiation process [52]. It is believed that inhomogeneous lithiation of the electrode would lead to a memory-effect when charge or discharge is not complete, because of the non-usage of some active material grains. A similar behavior was observed by Dubarry et al. [53] on under-charged $LiNi_{0.8}Co_{0.15}Al_{0.05}O_2$ electrodes. When $LiFePO_4$ electrode is cycled with $Li_4Ti_5O_{12}$ as negative electrode, this behavior could cause the lowering of cell capacity, even if the electrode intrinsic capacity is not changed.

5. Conclusion

$Li_4Ti_5O_{12}$/$LiFePO_4$ cells (in $LiPF_6$/EC:DMC) were aged by cycling, so that high degradation in term of capacity fade was observed after 4–5 months. Both electrodes were then analyzed using complementary electrochemical, spectroscopic and microscopic tools. The combination of all these techniques allowed to draw two conclusions on the degradation diagnosis:

1. No degradation in the composite electrode resulted from this aging, so that both electrodes could be used separately after aging with results similar to fresh ones.
2. Cell capacity fade resulted from internal imbalance in the cell, which may have been caused by parasitic reactions leading to a rich surface chemistry.

Those conclusions are inline with literature knowledge on $Li_4Ti_5O_{12}$ and $LiFePO_4$ active materials. Both remain attractive electrode materials due to their intrinsic stability, however it is of prime importance to better understand and lower parasitic reactions at the various interfaces in the cell.

Acknowledgment

This work was supported by the project PERLE2 of the Région Pays-de-la-Loire (France) and by CEA/Liten. The authors thank P.

Soudan and A. Thepaut for fruitful talks on electrochemistry and XRD results.

References

[1] The Boston Consulting Group, Batteries for Electric Cars. Challenges, Opportunities, and the Outlook to 2020, 2010.
[2] M. Safari, C. Delacourt, J. Electrochem. Soc. 158 (2011) A1123.
[3] B. Liaw, E. Roth, R. Jungst, G. Nagasubramanian, H. Case, D. Doughty, J. Power Sources 119-121 (2003) 874.
[4] M. Kassem, J. Bernard, R. Revel, S. Pélissier, F. Duclaud, C. Delacourt, J. Power Sources 208 (2012) 296.
[5] J. Vetter, P. Novák, M. Wagner, C. Veit, K.-C. Möller, J. Besenhard, M. Winter, M. Wohlfahrt-Mehrens, C. Vogler, A. Hammouche, J. Power Sources 147 (2005) 269.
[6] J. Christensen, J. Newman, J. Electrochem. Soc. 152 (2005) A818.
[7] C. Delacourt, M. Safari, J. Electrochem. Soc. 159 (2012) A1283.
[8] A. Barré, B. Deguilhem, S. Grolleau, M. Gérard, F. Suard, D. Riu, J. Power Sources 241 (2013) 680.
[9] L. Castro, R. Dedryvère, J.-B. Ledeuil, J. Bréger, C. Tessier, D. Gonbeau, J. Electrochem. Soc. 159 (2012) A357.
[10] M. Kassem, C. Delacourt, J. Power Sources 235 (2013) 159.
[11] L. Bodenes, R. Naturel, H. Martinez, R. Dedryvère, M. Menetrier, L. Croguennec, J.-P. Pérès, C. Tessier, F. Fischer, J. Power Sources 236 (2013) 265.
[12] M.H. Kjell, S. Malmgren, K. Ciosek, M. Behm, K. Edström, G. Lindbergh, J. Power Sources 243 (2013) 290.
[13] K. Amine, J. Liu, I. Belharouak, Electrochem. Commun. 7 (2005) 669.
[14] K. Striebel, J. Shim, A. Sierra, H. Yang, X. Song, R. Kostecki, K. McCarthy, J. Power Sources 146 (2005) 33.
[15] M. Koltypin, D. Aurbach, L. Nazar, B. Ellis, J. Power Sources 174 (2007) 1241.
[16] D. Aurbach, B. Markovsky, G. Salitra, E. Markevich, Y. Talyossef, M. Koltypin, L. Nazar, B. Ellis, D. Kovacheva, J. Power Sources 165 (2007) 491.
[17] M. Herstedt, M. Stjerndahl, A. Nytén, T. Gustafsson, H. Rensmo, H. Siegbahn, N. Ravet, M. Armand, J. Thomas, K. Edström, Electrochem. Solid-state Lett. 6 (2003) A202.
[18] K. Edström, T. Gustafsson, J. Thomas, Electrochimica Acta 50 (2004) 397.
[19] M. Koltypin, D. Aurbach, L. Nazar, B. Ellis, Electrochem. Solid-state Lett. 10 (2007) A40.
[20] N. Dupré, J.-F. Martin, J. Degryse, V. Fernandez, P. Soudan, D. Guyomard, J. Power Sources 195 (2010) 7415.
[21] P. Prosini, Solid State Ionics 144 (2001) 185.
[22] D. Abraham, E. Reynolds, E. Sammann, A. Jansen, D. Dees, Electrochimica Acta 51 (2005) 502.
[23] D.P. Abraham, E.M. Reynolds, P.L. Schultz, A.N. Jansen, D.W. Dees, J. Electrochem. Soc. 153 (2006) A1610.
[24] J. Shu, Electrochem. Solid-state Lett. 11 (2008) A238.
[25] C. Koga, S. Wada, M. Nakayama, Electrochimica Acta 55 (2010) 2561.
[26] S. Franger, C. Bourbon, F. Le Cras, J. Electrochem. Soc. 151 (2004) A1024.
[27] A. Jaiswal, C.R. Horne, O. Chang, W. Zhang, W. Kong, E. Wang, T. Chern, M.M. Doeff, J. Electrochem. Soc. 156 (2009) A1041.
[28] Revision 2, United States Advanced Battery Consortium, Electric Vehicle Battery Test Procedures Manual, 1996.
[29] N. Dupré, J. Oliveri, J. Degryse, J.-F. Martin, D. Guyomard, Ionics 14 (2008) 203.
[30] K. Zaghib, M. Dontigny, A. Guerfi, P. Charest, I. Rodrigues, A. Mauger, C. Julien, J. Power Sources 196 (2011) 3949.
[31] D. Abraham, J. Knuth, D. Dees, I. Bloom, J. Christophersen, J. Power Sources 170 (2007) 465.
[32] M. Maccario, L. Croguennec, F. Le Cras, C. Delmas, J. Power Sources 183 (2008) 411.
[33] M.C. Tucker, M.M. Doeff, T.J. Richardson, R. Finones, J.A. Reimer, E.J. Cairns, Electrochem. Solid-state Lett. 5 (2002) A95.
[34] B.M. Meyer, N. Leifer, S. Sakamoto, S.G. Greenbaum, C.P. Grey, Electrochem. Solid-state Lett. 8 (2005) A145.
[35] A.V. Plakhotnyk, L. Ernst, R. Schmutzler, J. Fluor. Chem. 126 (2005) 27.
[36] G. Zhang, C.E. Shaffer, C.-Y. Wang, C.D. Rahn, J. Electrochem. Soc. 160 (2013) A2299.
[37] P. Svens, M. Kjell, C. Tengstedt, G. Flodberg, G. Lindbergh, Energies 6 (2013) 400.
[38] K. Wu, J. Yang, Y. Liu, Y. Zhang, C. Wang, J. Xu, F. Ning, D. Wang, J. Power Sources 237 (2013) 285.
[39] J.C. Burns, N.N. Sinha, G. Jain, H. Ye, C.M. VanElzen, E. Scott, A. Xiao, W.M. Lamanna, J.R. Dahn, J. Electrochem. Soc. 161 (2014) A247.
[40] D. Guy, B. Lestriez, D. Guyomard, Adv. Mater. 16 (2004) 553.
[41] M. Cuisinier, N. Dupr, P. Moreau, D. Guyomard, J. Power Sources 243 (2013) 682.
[42] J.E. Harlow, D.A. Stevens, J.C. Burns, J.N. Reimers, J.R. Dahn, J. Electrochem. Soc. 160 (2013) A2306.
[43] M. Dubarry, C. Truchot, B. Liaw, K. Gering, S. Sazhin, D. Jamison, C. Michelbacher, J. Power Sources 196 (2011) 10336.
[44] S. Krueger, R. Kloepsch, J. Li, S. Nowak, S. Passerini, M. Winter, J. Electrochem. Soc. 160 (2013) A542.
[45] A.J. Smith, J.C. Burns, J.R. Dahn, Electrochem. Solid-state Lett. 13 (2010) A177.
[46] D. Aurbach, J. Electrochem. Soc. 143 (1996) 3809.
[47] D. Aurbach, K. Gamolsky, B. Markovsky, G. Salitra, Y. Gofer, U. Heider, R. Oesten, M. Schmidt, J. Electrochem. Soc. 147 (2000) 1322.
[48] V. Eshkenazi, E. Peled, L. Burstein, D. Golodnitsky, Solid State Ionics 170 (2004) 83.
[49] M. Cuisinier, J.F. Martin, P. Moreau, T. Epicier, R. Kanno, D. Guyomard, N. Dupré, Solid State Nucl. Magn. Reson. 42 (2012) 51–61.
[50] N. Delpuech, N. Dupré, D. Mazouzi, J. Gaubicher, P. Moreau, J. Bridel, D. Guyomard, B. Lestriez, Electrochem. Commun. 33 (2013) 72.
[51] N. Dupré, J.-F. Martin, J. Oliveri, P. Soudan, D. Guyomard, A. Yamada, R. Kanno, J. Electrochem. Soc. 156 (2009) C180.
[52] M. Katayama, K. Sumiwaka, R. Miyahara, H. Yamashige, H. Arai, Y. Uchimoto, T. Ohta, Y. Inada, Z. Ogumi, J. Power Sources (2014) in press, http://dx.doi.org/10.1016/j.jpowsour.2014.03.066.
[53] M. Dubarry, V. Svoboda, R. Hwu, B.Y. Liaw, J. Power Sources 165 (2007) 566.